Biophysical Chemistry, 46 (1993) 117–129
Elsevier Science Publishers B.V., Amsterdam

BIOCHE 01725

Distribution of the iron–heme displacement as resulting from myoglobin conformational substates: An AOM approach to the interpretation of the EPR spectra

Anna Rita Bizzarri [a], Mauro Bacci [b] and Salvatore Cannistraro [a,c,*]

[a] *Unità INFM-CNR, Dipartimento di Fisica dell'Università, Perugia I-06100 (Italy)*
[b] *Istituto di Ricerca sulle Onde Elettromagnetiche del CNR, Firenze (Italy)*
[c] *Dipartimento di Scienze Ambientali, Sezione Chimica e Fisica, Università della Tuscia, Viterbo (Italy)*

(Received 17 August 1992; accepted in revised form 30 September 1992)

Abstract

The electron paramagnetic resonance (EPR) low-temperature spectra of high spin ferric myoglobin samples in different solvent composition have been analyzed in terms of a distribution of the energy differences Δ_1 and Δ_2 for the iron low-lying electronic states. The widths of these distributions, which are found to be dependent on the solvent composition, have been correlated to the presence of a frozen ensemble of conformational substrates. A dedicated analysis based on the angular overlap method (AOM) has allowed us to work out a quantitative relationship between the Δ_1 and Δ_2 distributions and the spread of the iron–heme displacement; this being a structural parameter relevant for the biological functionality of the protein. The observed dependence of the iron–heme displacement distribution on the solvent composition is discussed.

Keywords: Myoglobin; Conformational substates; Electronic paramagnetic resonance; Angular overlap method

1. Introduction

Proteins as other complex systems like glasses and spin glasses show characteristic anomalies in their low temperature thermal, dielectric and electron paramagnetic resonance (EPR) properties [1–4]. Such a peculiar behaviour could be connected to the presence of an ensemble of nearly isoenergetic substates belonging to a wide configurational space [5,6]. These conformational substrates (CS) seem to play an important role in the biological functionality of the proteins [7]. Actually, at physiological temperature, proteins fluctuate among CS; such a behaviour affecting the kinetic response of the molecules [8,9]. A possible connection between the multiple time scale processes, which characterize the dynamical behaviour of proteins [10], and the transitions among the CS is still object of debate [11,12].

By decreasing the temperature, the fluctuations among CS tend to vanish, until the protein solution undergoes, at T_g, a glass-like transition below which the biomolecules appear to be frozen

* Corresponding author.

in many CS whose distribution may be modulated by external agents such as pressure, pH and solvents [13–15]; the overall organization of the system being reminiscent of the quenched disorder present in amorphous materials [16].

Myoglobin (Mb), one of the most studied proteins, is a sort of laboratory to investigate the relationship among CS, dynamics and functionality. Many different experimental and theoretical resources have been employed to reach a complete understanding of the overall protein behaviour [17–26]. An X-ray diffraction analysis of the low temperature Mb samples points out a significant mean square displacement $\langle x^2 \rangle$ for both the backbone and side-chain atoms, such an effect arising from the presence of a frozen ensemble of molecules in different CS [27]. On the other hand, most of the techniques employed to study the CS in this protein have been mainly focused on the structural and dynamical aspects of the active site which is constituted by the iron heme prosthetic group.

The CO-rebinding kinetics studies performed on Mb at different temperatures by optical spectroscopy [5,7,15] (and using a large amount of added glycerol or ethylene glycol to make the samples transparent) show a non-exponential time response of the system. Such a behaviour has been interpreted in terms of a distribution in the enthalpy barriers involved in the rebinding process and possibly connected to a distribution of some structural parameters related to the iron–ligand binding [21]. In this connection, a crucial role seems to be played by the iron–heme displacement which has been found to show a significant spread around its average value [28]. In this context, it is reasonable to suppose that such a spread could be related to the presence of the CS distribution [28]; the proximal histidine acting as a link between the prosthetic group and the remaining portion of the molecule [29].

In the present paper EPR spectroscopy, which is very sensitive in detecting even subtle changes in the microenvironment of paramagnetic ions and which has been shown to be particularly suitable to investigate the presence of CS distribution [4,26,30–34], has been applied to high spin ferric Mb frozen solutions in order to better assess the relationship between the presence of a Mb molecule CS distribution and the spread in the iron–heme displacement. The EPR spectra of the paramagnetic Mb samples in different solvent composition, have been analyzed by computer simulation in the framework of a statistical model assuming a Gaussian distribution of the two iron crystal field parameters Δ_1 and Δ_2 (see below). The widths of these distributions, which were found to be significantly dependent on the solvent composition, have been put into relationship to the presence of a CS distribution in Mb. To work out a quantitative relationship between the Δ_1 and Δ_2 distributions and the iron-heme displacement distribution, we have applied, for the first time, the angular overlap method (AOM), which is a zero-th order molecular orbital approximation particularly suitable in low symmetry metal complexes to determine the energy dependence from the bond angles to the high spin ferric heme.

The results point out that the addition of glycerol, ethylene glycol and the presence, in the solution, of sucrose can induce a significant narrowing of the iron–heme displacement distribution.

The paper is organized as follows. In Section 2, the experimental methods and the method employed to analyze the EPR spectra of ferric Mb are reported. In Section 3, the EPR results for Mb samples in different solvent composition are presented. Section 4 describes the approach based on the AOM to interpret the EPR results in terms of a spread of the iron–heme displacement. The distribution of the iron–heme displacement and its dependence on the solvent composition are discussed in Section 5. Finally, conclusions are presented in Section 6.

2. Materials and EPR spectral analysis

Myoglobin EPR samples were prepared by dissolving commercial (Sigma Chem. Co.) lyophilized horse skeletal muscle Mb in 0.2 *M* phosphate buffer. The highest concentration of Mb in the solutions was about 5 m*M*. Final pH for the Mb solutions was 6.8. Ferricyanide was used to oxi-

dize the heme iron to the ferric valence state and the solutions were dialysed several times against buffers to remove the oxidant. Samples in the presence of the two organic solvents, glycerol (Gly) or ethylene glycol (EthGly), have been prepared in 1:1 (by volume) water–solvent mixture. Samples in presence of sucrose (Sucro) have been prepared in 1:1 water–sucrose (1 *M* solution) mixture. All chemicals used were of analytic reagent grade.

All the EPR spectra were recorded at 77 K (liquid nitrogen) by an X-band Varian E109 spectrometer. A fast cooling rate procedure (fast) was performed by dipping the samples into liquid nitrogen. To calculate the experimental *g*-values, a magnetic field calibration was performed with a Magnion Precision NMR Gaussmeter Mod. G-542; the microwave frequency being measured with a Marconi 2440 counter.

The acquisition of EPR data was carried out on a HP 86A personal computer through a home made interface connected to a IEEE 488 bus [35]. To run both simulations and "best fit" programs, the same microcomputer was switched to an intelligent terminal of the main frame computer (VAX 8350), through a serial interface and an HP terminal emulator.

It is well-known that the EPR spectra at 77 K of aqueous samples of ferric–Mb at pH ~ 7 are characterized by two resonances, one at $g \simeq 6$ and a weaker one at $g \simeq 2$ [36]. The weak ligand H_3O^+ to the sixth coordination site of iron determines a high spin state, $S = 5/2$. In tetrahedral or lower symmetry fields, the system, characterized by the $^6A_1$ state, retains its six-fold degeneracy even when spin–orbit coupling is considered to first order, but, in second order, the degeneracy is lifted to give three Kramers doublets.

In the presence of a magnetic field, the system can be described by a second order spin Hamiltonian

$$H_s = g_e \beta \boldsymbol{H} \cdot \boldsymbol{S} + D\left[S_z^2 - S(S+1)/3\right] + E\left(S_x^2 - S_y^2\right) \qquad (1)$$

where g_e is the value for the free electron; D and E are the tetragonal and the rhombic zero-field splittings, respectively. For heme proteins, the condition of large zero field splitting is satisfied ($D \sim 10\ \mathrm{cm}^{-1}$) [36] and only transitions within the lowest Kramers doublet occur; a fictitious spin $S = 1/2$ can then be used to fully represent the spin Hamiltonian of the system, which for axial symmetry ($g_x = g_y = g_\perp$ and $g_z = g_\parallel$) can be expressed by

$$H_s' = g_\parallel \beta H_z S_z + g_\perp \beta \left(H_x S_x + H_y S_y\right) \qquad (2)$$

where $g_\parallel \simeq 2$ and $g_\perp \simeq 6$ are the *g*-values which are observed in the experimental spectra. Splitting of the in-plane value into two values, g_x and g_y, may result in a broadening (as in our case) or even in a splitting [37] of the $g \simeq 6$ line. High order corrections, arising from spin–orbit mixing of the excited quartet states into the lowest Kramers doublet lead, under the assumption of a four-state model [26,31,38–40], to the following expression for g_x and g_y

$$g_{x,y} = 6.01 \pm 24\frac{E}{D} - 18.7\left(\frac{E}{D}\right)^2 - 12\eta^2 \qquad (3)$$

where the tetragonal zero-field splitting D is given by

$$D = \frac{\xi^2}{5}\left(\frac{1}{\Delta_1} - \frac{1}{\Delta_2}\right) \qquad (4)$$

and the rhombic zero-field splitting E

$$E = \frac{1}{10}\frac{\gamma \xi^2}{\Delta_2^2} \qquad (5)$$

the spin–orbit mixing of excited quartet states into the lowest Kramers doublet is

$$\eta^2 = \frac{\xi^2}{5}\left(\frac{1}{\Delta_1^2} + \frac{1}{\Delta_1 \Delta_2} + \frac{1}{\Delta_2^2}\right) \qquad (6)$$

ξ is the effective spin–orbit coupling constant ($\xi \sim 300\ \mathrm{cm}^{-1}$) which is reduced from the free-ion value ($\xi \sim 420\ \mathrm{cm}^{-1}$); Δ_1, Δ_2, and γ are the energy differences between the low-lying electronic states of high ferric heme (see Fig. 1). In a general way, the derivative field-swept EPR absorption spectrum, related to randomly oriented

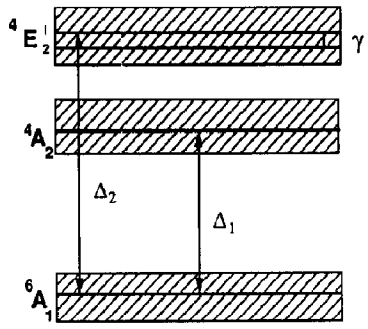

Fig. 1. Energy level diagram of the low-lying electronic states of high spin ferric heme. The shaded regions indicate the variability of the energy levels (not in scale).

paramagnetic centers with $S = 1/2$, can be reproduced by the expression [41]

$$\frac{dS(\nu_c, H)}{dH} = C\frac{\nu_c h}{\beta}\int_0^{\frac{\pi}{2}}\int_0^{\frac{\pi}{2}}\frac{P(\theta,\phi)}{g(\theta,\phi)} \times \frac{df([H-H_0],\sigma_H)}{dH}\sin\theta\, d\theta\, d\phi \tag{7}$$

where the $1/g(\theta, \phi)$ is the Aasa–Vanngard [42] correction C is a constant that encompasses all instrumental parameters, $P(\theta, \phi)$ is the orientation dependent transition probability which for an $S = \frac{1}{2}$ system can be exactly expressed by [43]

$$P(\theta,\phi) = g_x^2 + g_y^2 + g_z^2 - \frac{1}{g^2(\theta,\phi)} \times \left[g_x^4 \sin^2\theta\cos^2\phi + g_y^4 \sin^2\theta \sin^2\phi + g_z^4 \cos^2\theta\right] \tag{8}$$

$f([H - H_0], \sigma_H)$ is the lineshape function (connected to the residual linewidth [44]) centered at the resonance field H_0 and with a linewidth parameter σ_H measured in field units. In the shown simulations a Lorentzian lineshape, with $\sigma_H = 25$ gauss [26], has been employed. The integration over θ and ϕ in eq. (7) takes into account for the random orientation of the molecular axes with respect to the magnetic field.

According to the Isomoto algorithm [43], once the values of the **g**-tensor have been fixed, the resonance field H_0 can be calculated at each orientation (θ, ϕ) and the spectrum is computer-generated by carrying on the integration in eq. (7) as a sum over θ (in step of one degree) and over ϕ (in step of three degrees). The increment values for θ and ϕ have been chosen in order to limit the computer noise to a level lower than that corresponding to the experimental errors. It is known, however, that the EPR spectra of metallo-proteins are characterized by a large inhomogeneous broadening (**g**-strain) which is superimposed on all the other broadening effects [4,33,45–52]. According to previous papers [26,30–34,40], we assume that the presence of frozen CS distribution entails a distribution of crystal field parameters which in turn could be responsible for the spread in the **g**-tensor values. On such a ground, we have simulated our spectra by assuming that the crystal field parameter Δ_1 and Δ_2 are distributed around a mean value (Fig. 1). In particular, two independent gaussian distributions for Δ_1 and Δ_2 have been introduced in the simulation method; so that the resulting simulated spectrum can be visualized as a superposition, weighed in a proper way, of different spectra each related to different values of (g_x, g_y, g_z) [26,30]. The simulated EPR derivative spectrum can be finally expressed by

$$\frac{dS(\nu_c, H)}{dH} = \frac{C\nu_c h}{\beta}\frac{1}{2\pi\sigma_{\Delta_1}\sigma_{\Delta_2}}\iint\frac{dS(\nu_c, H, \Delta_1, \Delta_2)}{dH} \times \exp\left(-\left[\frac{\Delta_1 - \Delta_1^0}{\sigma_{\Delta_1}}\right]^2\right) \times \exp\left(-\left[\frac{\Delta_2 - \Delta_2^0}{\sigma_{\Delta_2}}\right]^2\right) d\Delta_1\, d\Delta_2 \tag{9}$$

where, assigned Δ_1 and Δ_2 (and therefore g_x and g_y), the corresponding derivative spectrum $dS(\nu_c, H, \Delta_1, \Delta_2)/dH$ is determined by means of eq. (7).

The computer-synthesized spectra have then been used to fit the experimental EPR spectra in order to determine the parameters Δ_1^0, Δ_2^0, σ_{Δ_1} and σ_{Δ_2} characterizing the corresponding gaussian distributions. The bestfit is obtained by a minimization procedure of the χ^2-function

$$\chi^2 = \sum_{i=1}^{N} \left[\frac{I^{\exp}(H_i) - I^{\sin}(H_i,p)}{\sigma_i} \right]^2 \qquad (10)$$

where $I^{\exp}(H_i)$ is the derivative of the experimental EPR absorption spectrum sampled at 200 discrete points of the magnetic field, $I^{\sin}(H_i, p)$ is the simulated spectrum that also depends on the parameter set (Δ_1^0, Δ_2^0, σ_{Δ_1} and σ_{Δ_2}), and σ_i is the standard deviation calculated for the ith experimental point of the EPR spectrum by repeated runs. The search of the bestfit parameters has been done by following a simulated annealing approach [53]; each parameter having been allowed to vary over a wide range consistent with both those estimated from the experimental spectra and those reported in the literature [40].

3. EPR results

The experimental EPR spectra of Mb samples in different conditions, restricted around the most significant region ($g \simeq 6$), are shown in Fig. 2; the corresponding simulated spectra (dashed lines) obtained by means of eq. (9) are also shown. The agreement between the experimental and the simulated patterns appears very good; however the goodness of the fit has been confirmed, in each case, by the χ^2-test.

The parameters Δ_1^0, σ_{Δ_1}, Δ_2^0, and σ_{Δ_2} as obtained by the simulation of the EPR spectra are reported in Table 1. The physical soundness of the simulations performed is assessed by the fact that the values of the Δ_1 and Δ_2 distributions are in agreement with the related experimental values reported in literature [40].

Table 1 shows that the analyzed EPR spectra are characterized by a significant spread in the crystal field parameters Δ_1 and Δ_2; such a spread being expressed by the relatively large values resulting for the σ_{Δ_1} and σ_{Δ_2} parameters. Both

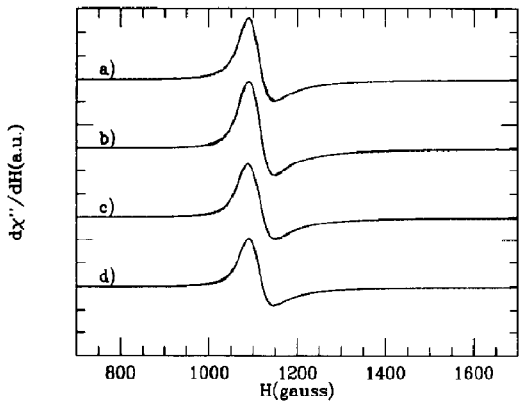

Fig. 2. Experimental (continuous line) and simulated (dashed line) X-band EPR spectra, recorded at 77 K, restricted to the $g = 6$ region of high spin ferric Mb samples in different conditions: (a) Mb aqueous solutions, (b) Mb aqueous solutions in presence of glycerol (1:1 by volume), (c) Mb aqueous solutions in presence of ethylene glycol (1:1 by volume), and (d) Mb aqueous solutions with added sucrose (1 M).

the Δ_1 and Δ_2 distributions result to be affected by the presence of glycerol, ethylene glycol and sucrose in the Mb solutions; however, the Δ_2 distribution appears to be the most sensitive parameter to changes occurring in the solvent composition. It should be noted that these observed solvent-induced effects are to be attributed to a bulk modification, since the presence of glycerol, ethylene glycol and sucrose in small amounts (less than 1:1 heme molar concentration) does not induce any change in the EPR spectra of Mb samples (results not shown). On the other hand,

Table 1

Central values and the root of the corresponding variances of the gaussian distributions related to the crystal field parameters Δ_1 and Δ_2. These values have been obtained by simulations of the $g \simeq 6$ line of the EPR spectra, recorded at 77 K, of Mb aqueous solutions in different conditions. The 68% confidence limits, extracted by the fitting procedure, are given, in percentage, by 0.5% for Δ_1^0, 3% for σ_{Δ_1}, 0.5% for Δ_2^0 and 5% for σ_{Δ_2}.

Sample	Δ_1^0 (cm^{-1})	σ_{Δ_1} (cm^{-1})	Δ_2^0 (cm^{-1})	σ_{Δ_2} (cm^{-1})
Mb (Fast)	2266	259	5759	936
Mb + Gly (Fast)	2194	280	5500	549
Mb + EthGly (Fast)	2248	248	5422	619
Mb + Sucro (Fast)	2181	231	5646	625

it is known that addition, in small quantities, of some alcohols, like methanol and ethanol, which directly bind to the heme group significantly modifies the EPR spectra of heme-proteins [31,54].

For the Δ_1 distribution, it can be observed a reduction of the Δ_1^0 parameter of about 3.2%, 0.8% and 3.8%, with respect to pure Mb solutions, for samples in presence of glycerol, ethylene glycol and sucrose, respectively; on the other hand, σ_{Δ_1} increases of 8% in presence of glycerol, while it decreases of 4.2% in presence of ethylene glycol and of 11% in presence of sucrose.

Concerning the Δ_2 distribution, Δ_2^0 and σ_{Δ_2} always decrease with respect to pure Mb solution, as consequence of the solvent addition; in particular, Δ_2^0 decreases of 4.5%, 5.8% and 2% while σ_{Δ_2} decreases of 41%, 34% and 33% for samples in presence of glycerol, ethylene glycol and sucrose, respectively.

4. Analysis of the EPR results by following an AOM approach

The analysis of the EPR spectra of Mb samples with different added solvents points out the presence of a significant spread in the crystal field parameters Δ_1 and Δ_2. This spread reflects the degree of heterogeneity of the microenvironment around the metal ion, and it should be interpreted in terms of a distribution of the structural parameters characterizing the heme-complex. For that purpose, a suitable approach could be represented by the AOM which can be fruitfully employed to determine the ligand field splitting of the Fe^{3+} d-orbitals, where small variations of the arrangement of the ligands around the central ion [55] could be evaluated. The AOM takes its name and gains its power by representing the overlap integral S between two orbitals as a simple product of radial and angular terms

$$S = S_\lambda(r) F_{\lambda,\omega} \tag{11}$$

The diatomic overlap integral $S_\lambda(r)$ depends upon the interatomic distance, the nature of atoms and the types of orbitals; λ indicates the bonding symmetry with respect to the metal–ligand axis (σ, π or δ), and ω specifies the particular orbital for $\lambda > 0$. The angular term $F_{\lambda,\omega}$ is a simple function of the angular polar coordinates θ, ϕ of one atom relative to another; it is a fraction of the maximum overlap which occurs for colinear atoms, different functions being found for different values of λ.

It can be shown [56] that the energy change, e_λ, of a given metal orbital, as induced by the interaction with a ligand, is

$$e_\lambda = K_\lambda S_\lambda^2 F_{\lambda\omega}^2 \tag{12}$$

In the Wolfsberg–Helmholtz approximation [57], the K_λ constant results to be

$$K_\lambda \simeq \frac{H_L}{H_M - H_L} \tag{13}$$

where H_M and H_L are the metal and ligand orbital energies, respectively.

If the ligand is not lying on the Z-axis, a rotation of the coordinate system is required. Under the assumption that the effects of different ligands are additive and that the ligand–ligand overlap can be neglected, the general ligand field matrix element can be expressed as [58]

$$\langle \phi_i | V | \phi_j \rangle = \sum_{\lambda\omega} \sum_{n}^{N} e_{\lambda n} F_{\lambda\omega}(\phi_i, X_n) F_{\lambda\omega}(\phi_j, X_n) \tag{14}$$

where V is the potential induced by the ligands; the first sum on the metal orbitals is referred to a coordinate system $x'y'z'$ such that the i-ligand is on the z'-axis; the second sum is extended to the N ligands X_n. $F_{\lambda\omega}(\phi_i, X_n)$ and $F_{\lambda\omega}(\phi_j, X_n)$ are the columns of the AOM rotation matrix which relates the metal orbitals in the primed and unprimed coordinate system (for the angular dependence of the Overlap integrals see (Tables in ref. [56]).

In order to evaluate the matrix elements in eq. (14), for each ligand three independent parameters, e_σ, e_π and e_δ, are required (or even five, if the two components $\pi_s\pi_c$ and $\delta_s\delta_c$ of the π or δ symmetry are considered). In our case, it seems feasible to neglect δ bond effects, and, if, at first approximation, we put $e_{\pi s} = e_{\pi c} = e_\pi$, only two

parameters for each ligand can be used [56]. In general, the semiempirical parameters e_λ could be theoretically evaluated or deduced from experimental data [59]. It should be noted that the energy differences of the low-lying electronic states Δ_1 and Δ_2 can be expressed in terms of two different contributes [60]: (i) the splitting of the *d*-orbitals, induced by the presence of the ligand field assessable through the AOM; (ii) the electrostatic contribute that can be expressed in terms of the Racah parameters B and C. From the definition of Δ_1 and Δ_2 (see Fig. 1), it follows

$$\Delta_1 = E(^4A_2) - E(^6A_1)$$
$$= [E(\zeta) - E(\epsilon)] + [22B + 7C] \quad (15)$$

and

$$\Delta_2 = E(^4E) - E(^6A_1)$$
$$= \tfrac{1}{2}\{[21B + 10C]\} + \tfrac{1}{2}\{[E(\eta) - E(\theta)] + \tfrac{1}{4}[E(\xi) - E(\epsilon)]\} \quad (16)$$

where the symbols ξ, η, ζ, θ and ϵ stand for the one electron levels d_{yz}, d_{xz}, d_{xy}, d_{z^2}, and $d_{x^2-y^2}$, respectively. For the Racah parameters, the values $B \simeq 500$ cm^{-1} (for the free ion $B = 1015$ cm^{-1}) and $C = 4.4B$ ($C \simeq 2200$ cm^{-1}) have been used; these values being within the allowed range for iron complexes [61].

In order to evaluate the splitting of the *d*-orbitals by means of the AOM, the geometrical arrangement of the heme group should be assigned. It is known that the heme complex in metMb is a six-coordinate compound arranged in tetragonal symmetry with a small rhombic distortion, in which the metal ion is displaced out of the heme-plane to the proximal histidine side of a quantity, *a*, of 0.40 Å [62]. Accordingly, a simplified geometry for the heme structure (see Fig. 3) has been assumed; in particular, the four ligands of the heme-plane have been considered as equivalent; moreover, the two axial ligands have been assumed to be along to the normal to the heme-plane. In this case, only six parameters, instead of twelve, are required in the evaluation of the Δ_1 and Δ_2 values by means of the AOM. The following symbols for the AOM parameters

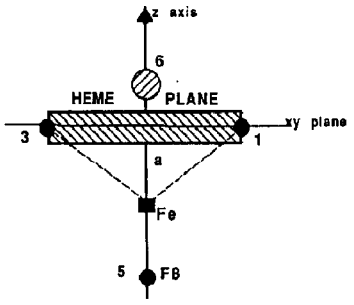

LIGAND	θ	φ
1	90°	0°
2	90°	90°
3	90°	180°
4	90°	270°
5	180°	0°
6	0°	0°

Fig. 3. Geometrical arrangement of the ligands around the metal ion in the heme-complex. θ and ϕ represent the angle values employed in the AOM approach for each ligand.

have been employed: e_σ^{I} and e_π^{I}, to describe the four equivalent ligands of the heme-plane; e_σ^{II} and $e^{\mathrm{I}}{}_\pi$, to describe the ligand in fifth position, i.e. the N atom of the imidazole belonging to the proximal histidine; finally, e_σ^{III} and e_π^{III} have been associated to the ligand in the sixth position (i.e. the bound water molecule).

Some examples of the trend of Δ_1 and Δ_2, as function of the AOM parameters, e_σ^{I}, e_σ^{II}, e_σ^{III}, $(e_\pi/e_\sigma)^{\mathrm{I}}$, $(e_\pi/e_\sigma)^{\mathrm{II}}$ and $(e_\pi/e_\sigma)^{\mathrm{III}}$ for a fixed geometrical arrangement the system, are shown in Fig. 4 and Fig. 5. Figure 4 shows that an increase of the e_σ^{I} value yields a decrease of the Δ_1 and Δ_2 values; such an effect being more marked for Δ_1. On the contrary, Δ_1 is not affected by changes in the e_σ^{II} and e_σ^{III} values, while the Δ_2 value is lowered according to the sum of the e_σ^{II} and e_σ^{III} values. Figure 5 shows that an increase in the $(e_\pi/e_\sigma)^{\mathrm{I}}$ value causes an increase of both Δ_1 and Δ_2; moreover, Δ_1 is not influenced by $(e_\pi/e_\sigma)^{\mathrm{II}}$ and $(e_\pi/e_\sigma)^{\mathrm{III}}$ which, on the contrary, affect the Δ_2 values. Therefore, in general, it should be remarked that the changes of the ligands on the heme-plane can affect both the

Δ_1 and Δ_2 parameters, while changes of the ligands in axial position can only affect Δ_2.

On the basis of the above analysis, we have used for further calculations $e_\sigma^{I} \approx 10000\ cm^{-1}$, $e_\sigma^{II} \approx 2000\ cm^{-1}$ and $e_\sigma^{III} \approx 500\ cm^{-1}$. These values are slightly different from those used for Fe^{2+} [63], but the higher oxidation state of iron in the present case can make plausible the assumed values. Moreover, we have used $(e_\pi/e_\sigma)^{I} = 0.1$ and $(e_\pi/e_\sigma)^{II} = (e_\pi/e_\sigma)^{III} = 0.15$, as fixed values [63].

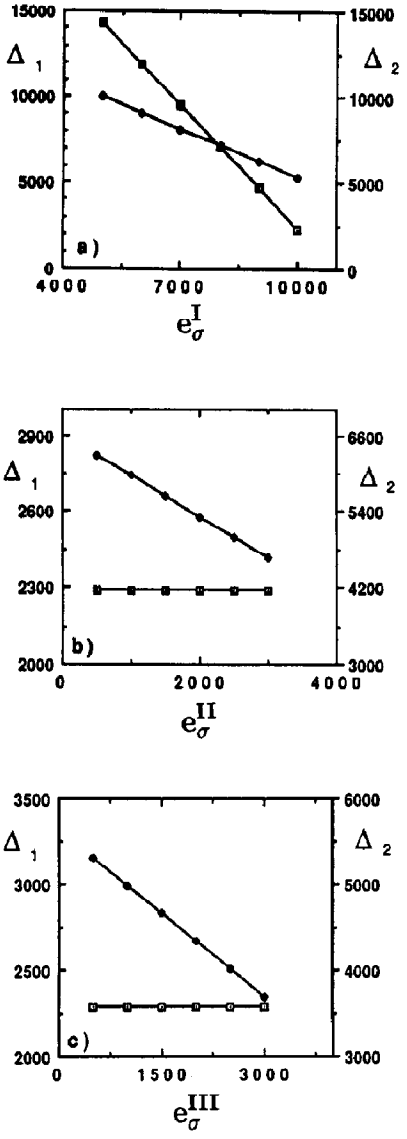

Fig. 4. Trends of Δ_1 (open symbols) and Δ_2 (full symbols) as function of the parameters: e_σ^{I} (a), e_σ^{II} (b), and e_σ^{III} (c). In each figure all the other AOM parameters are kept fixed: $e_\sigma^{I} = 10000\ cm^{-1}$, $e_\sigma^{II} = 2000\ cm^{-1}$, $e_\sigma^{III} = 500\ cm^{-1}$, $(e_\pi/e_\sigma)^{I} = 0.1$, $(e_\pi/e_\sigma)^{II} = 0.15$, and $(e_\pi/e_\sigma)^{III} = 0.15$.

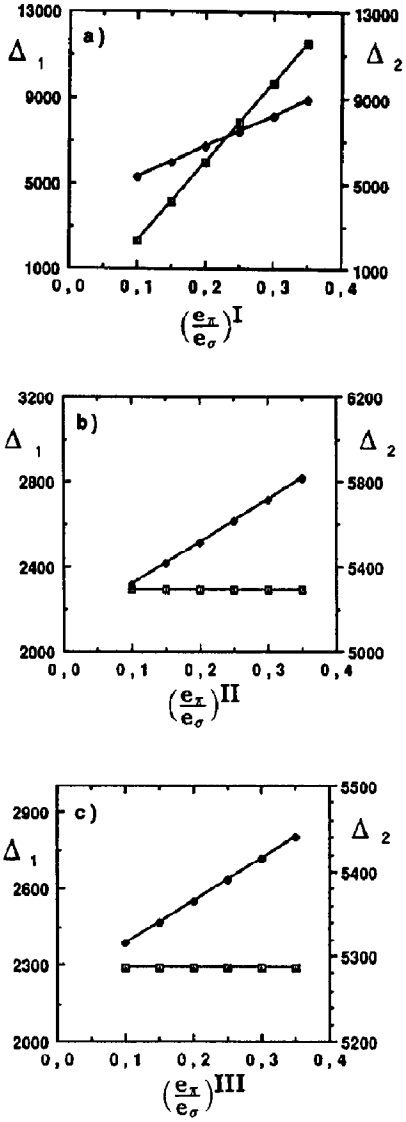

Fig. 5. Trends of Δ_1 (open symbols) and Δ_2 (full symbols) as function of the parameters: $(e_\pi/e_\sigma)^{I}$ (a), $(e_\pi/e_\sigma)^{II}$ (b), and $(e_\pi/e_\sigma)^{III}$ (c). In each figure all the other AOM parameters are kept fixed: $e_\sigma^{I} = 10000\ cm^{-1}$, $e_\sigma^{II} = 2000\ cm^{-1}$, $e_\sigma^{III} = 500\ cm^{-1}$, $(e_\pi/e_\sigma)^{I} = 0.1$, $(e_\pi/e_\sigma)^{II} = 0.15$ and $(e_\pi/e_\sigma)^{III} = 0.15$.

The variation of the central values Δ_1^0 and Δ_2^0 as induced by different added solvents, could be mainly attributed to changes which involve essentially ligands in both the fifth and the sixth posi-

tions. Accordingly, we have assumed that the e_σ^I values are equal for all the analyzed Mb samples and we have determined the mean values for the iron–porphyrin displacement in order to exactly reproduce the Δ_1^0 value. These values are reported in Table 2. Then, the e_σ^{II} and e_σ^{III} values have been adjusted to obtain the corresponding value for Δ_2^0.

The spread of the crystal field parameter distributions Δ_1 and Δ_2, due to the CS distribution [26], should be connected to the parameters characterizing the heme-group. The presence of a frozen ensemble of molecules assuming different CS, as it has been observed by X-ray diffraction [17,27], results into a significant mean-square displacement of each amino-acid residue [27]. Therefore, it could be expected that the ligand in the fifth position, which directly senses the presence of CS distribution, can modulate the metal ion position [29]. In this context, it has been observed that the proximal histidine shows a mean square displacement, $\langle x^2 \rangle$, of about 0.10 Å^2 [27]. On such a ground, it is reasonable to assume that, according to different positions of the proximal histidine, the iron is forced to assume different positions with respect to the heme-plane. We have tried to numerically reproduce the Δ_1 and Δ_2 distributions by introducing a Gaussian distribution for the iron position; this fact implies a change in the geometry of the system, i.e. in the values of the θ and ϕ angles and in the length of the iron-ligand bonds. A correction on the parameters e_σ^I, e_σ^{II}, e_σ^{III}, $(e_\pi/e_\sigma)^I$, $(e_\pi/e_\sigma)^{II}$ and $(e_\pi/e_\sigma)^{III}$ should moreover be introduced to take into account for the fact that an increase of the bond length causes a lowering of the angular overlap integral S; such a correction has been done in agreement with the indications reported in ref. [64].

Table 2

The values of the parameters, employed in the AOM approach. a_0 is the mean value for the iron–porphyrin displacement. e_σ^I is the AOM parameter concerning with the ligands on the heme-plane; e_σ^{II} and e_σ^{III} are the AOM parameters concerning with the fifth and the sixth ligand, respectively.

Sample	a_0 (Å)	e_σ^I (cm^{-1})	$(E_\sigma^{II} + e_\sigma^{III})$ (cm^{-1})
Mb (Fast)	0.400	10010	1954
Mb + Gly (Fast)	0.394	10010	2160
Mb + EthGly (Fast)	0.398	10010	2460
Mb + Sucro (Fast)	0.390	10010	1872

Table 3

Root of variances for the gaussian distributions of the iron-porphyrin displacement, a, as extracted from the results in Table 1 by a fit based on the AOM approach; σ_a^- concerns with the approach of iron to the heme-plane; σ_a^+ concerns with the departure of iron from the heme-plane; $\sigma_a = (\sigma_a^- + \sigma_a^+)/2$. The 68% confidence limits, extracted by the fitting procedure, are given, in percentage, by 5% for σ_a, 2% for σ_a^- and 2% for σ_a^+

Sample	σ_a (Å)	σ_a^- (Å)	σ_a^+ (Å)	σ_a^-/σ_a^+
Mb (Fast)	0.0575	0.0646	0.0504	1.28
Mb + Gly (Fast)	0.0325	0.0349	0.0302	1.16
Mb + EthGly (Fast)	0.0374	0.0404	0.0343	1.18
Mb + Sucro (Fast)	0.0385	0.0423	0.0346	1.22

To encompass the possibility of obtaining an asymmetrical distribution for the iron position, two different variances have been introduced to characterize the iron heme displacement distribution: one, $(\sigma_a^-)^2$, for the approach of the iron to the heme plane (negative displacement), and the other $(\sigma_a^+)^2$, for the removal from it (positive displacement).

The results obtained by the application of the AOM to the EPR results are reported in Table 3 while in Fig. 6 an example of the fit of the Δ_1 and Δ_2 distributions is shown. We have verified that small changes (less than 1%) did not result in significant variations of the iron–heme distribution (for details see ref. [29]). The σ_{a_0} value obtained for pure Mb solutions (0.0575Å) is to be compared with that of ferrous deoxy Mb. In this case, different experimental techniques provided somewhat different results: σ_a should fall within the interval 0.07 Å–0.3 Å [17,28,65,66]. The smaller value found for ferric Mb, can be justified by both the higher oxidation state for the iron and the presence of weaker ligand in the sixth position. The values of column 4 in Table 3 point out that a significant asymmetry is present in the distribution of the iron-porphyrin displacement. In particular, the iron moves closer to the heme

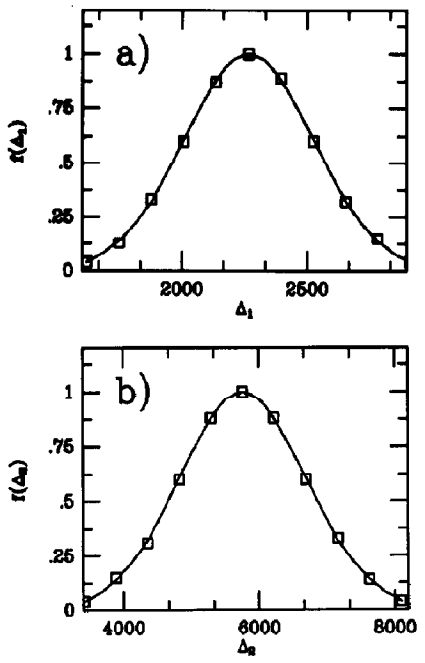

Fig. 6. The Gaussian distributions (continuous lines) of the crystal field parameters Δ_1 (a) and Δ_2 (b), corresponding to the central values Δ_1^0 and Δ_2^0 and to the variances σ_{Δ_1} and σ_{Δ_2}, of pure Mb sample, reported in Table 1. The fits (square symbols) have been derived from the AOM approach by using the parameters shown in Tables 2 and 3.

plane rather than to take away from it. From such an evidence, it could be speculated about the possibility that the presence of the sixth ligand, might in some way prevent the iron from performing large displacements towards the proximal histidine side.

It can be, moreover, observed that addition of large amount of glycerol, ethylene glycol and sucrose to Mb solutions, which causes a narrowing of the crystal field parameter distributions, results in a significant decrease in the σ_a value. This effect is more marked for samples with added glycerol, in which σ_a^- is lowered of 46% and σ_a^+ of 40%; while for ethylene and sucrose, σ_a^- is reduced of 37% and 34%, respectively; and σ_a^+ is reduced of 32% and of 31%. The ratio σ_a^-/σ_a^+ appears to be reduced in presence of glycerol, ethylene glycol and sucrose as compared with that of pure Mb, indicating a more symmetrical behaviour for the spread of the iron position as induced by these solvents.

5. Discussion

The use of the simulation method outlined in Section 4 has allowed us to extract the parameters characterizing the distribution of the ligand field energies Δ_1 and Δ_2 of Mb samples in different conditions. The fact that the central values (Δ_1^0 and Δ_2^0) of these distributions are found to be consistent with the experimental data reported in the literature and the goodness of the fits are indicative of the reliability of the computer model used.

The widths of the Δ_1 and Δ_2 distributions, as we have already mentioned, are to be discussed in close connection to the presence of the protein CS distribution [4,26,31,67]. Actually, frozen metallo-protein solutions, which are similar to glassy systems with respect to the microscopic disorder displayed by their structure, are characterized by the presence of a static ensemble of frozen CS. To such a conformational heterogeneity corresponds an heterogeneity in the orientation and/or position of the ligand groups that the protein molecule provides to the metal ion. Consequently, the Fe^{3+} ion ligand bonds are modulated (as regards the angles and the distances) according to the microenvironmental fluctuations.

The AOM approach has allowed us to correlated such a kind of heterogeneity in terms of a distribution of the iron–porphyrin displacement. Our results point out that, in high spin ferric Mb samples, the distance of iron from the hemeplane is distributed according to the presence of an ensemble of biomolecule structures representing the different CS. On the other hand, there are many experimental evidences supporting the fact that the iron position, in ferrous deoxy Mb, is distributed [8,17,28,65,66]. Therefore, the presence of the CS distribution affects, through the action of the proximal histidine, the iron position (with respect to the heme-plane). This results is particularly relevant to the biological functionality of the protein, in fact the iron-displacement is a parameter directly involved in the CO rebinding processes [8,28]. In particular, it can be assumed that the enthalpy barrier that the ligand in the heme-pocket has to overcome for rebinding

to the iron, is approximatively proportional to the iron–porphyrin displacement [28].

Tables 1 and 2 show that the presence of glycerol and ethylene glycol in large quantity yields a narrowing of the crystal field parameter distribution and also a decrease in the spread of the iron-porphyrin displacement. Since the iron ion is not directly exposed to the external solvent, the modifications induced by addition of these solvents should be attributed to a reduction in the heterogeneity of the strengths exercised by the proximal histidine onto the metal ion. In other words, the proximal histidine undergoes, in the presence of these solvents, to a weaker perturbation from other parts of the protein, affecting in a less significant way the metal ion position. These results can be directly interpreted in terms of a reduction in the heterogeneity in the CS distribution as induced by addition of these solvents. In general, it can be speculated about the fact that addition of glycerol, ethylene glycol and sucrose can cause modifications in the solvent properties, and than induce changes in the protein structure and also in the CS distribution. In particular, addition of glycerol, ethylene glycol and sucrose might be responsible for a damping of the protein motions; on the other hand, changes in the dielectric properties of the solvent, as induced by glycerol [68], could result into a different shielding of the amino-acid electrical charges, with subsequent modification in the interactions within the protein milieu. In addition to this effect, it has been observed that glycerol, which is preferentially excluded from the first hydration shell of the protein [69,70], causes a decrease in the hydrogen-bond-rupturing capacity of the medium [70] and then stabilizes the protein structure. Such a constraint on the dynamics of the solvent, could be responsible for the decreased number of accessible CS and for the decrease in the structural heterogeneity of the protein molecules observed in the presence of glycerol. A similar mechanism might be operative for what concerns protein solutions in the presence of ethylene glycol which shows chemico-physical properties similar to those of glycerol. Moreover, a similar constraint on the protein dynamics can be induced by sucrose which, however, is known to stabilize the protein structure through an increase in the water surface tension [71,72].

To assess which one of these molecular mechanisms is operative would requires a deeper investigation but, in any case, it should be remarked that modifications in the solvent properties might affect the CS distribution. In this context, it should be noted that data from rebinding kinetics experiments performed in presence of glycerol or ethylene glycol, should be revisited in the light of the present results.

Finally, it should be remarked that an additional source of structural heterogeneity could be represented by the strain imposed, on the protein structure, by the phase transition occurring in the solvent at the freezing point. These freezing-induced effects, which might be superimposed on other effects, are correlated to the ice-crystal dimensions and they can be minimized in the presence of some added solvents (glycerol, ethylene glycol) [48], or by submitting the samples to a slow cooling rate [4,26,67]. This phenomenon can affect, in a different way, various parts of the protein structure; for example, some artifacts in the ligand orientation and some modifications in the spin equilibrium have been observed according to the freezing procedure [73,74]. It would be possible that some contribution to the observed broadening of the crystal field parameter distributions might arise from the freezing process [21,75]; however, since slow cooling rate does not result in large changes [26], the main contribute should be attributed to an intrinsic heterogeneity of the system [31].

6. Conclusions

Owing to its high sensitivity in detecting microenvironmental fluctuations around the paramagnetic probes, EPR spectroscopy results to be a rewarding tool to investigate the structural and the dynamical properties of metallo-proteins; in particular, the analysis of the EPR spectral features can provide information on the presence of an ensemble of slightly different protein structures which are related to the CS. In this context, the AOM has revealed to be an helpful approach

to correlate the crystal field parameter distributions in ferric Mb, arising from the presence of such a CS distribution, to the spread of the iron-heme displacement. The iron position which results to be modulated, through the proximal histidine by the presence of the CS, has been found to be affected by the solvents which are usually used in the optical rebinding kinetics studies on Mb. It turns out that, as long as ferric Mb mimics ferrous Mb, EPR in a complementary technique to optical spectroscopy in order to study the CS distribution, and in particular to investigate the solvent-induced effects on the distribution and the correlated spread in the iron–heme displacement.

Acknowledgments

This work which has been done in partial fulfilment of the PhD thesis of one of the authors (A.R.B.), has been partially supported by CNR and MURST grants. One of us A.R.B. Acknowledges a fellowship issued by CNR Comitato Fisica.

References

1 I.S. Yang and A.C. Anderson, Phys. Rev. B34 (1986) 2942.
2 G.P. Singh, H.J. Schink, H.V. Lohneysen, F. Parak and S. Hunklinger, Z. Phys. B55 (1984) 23.
3 A.R. Drews, B.D. Thayer, H.J. Stapleton, G.C. Wagner, G. Giugliarelli and S. Cannistraro, Biophys. J, 57 (1990) 157.
4 S. Cannistraro, J. Phys. (France) 51 (1990) 131.
5 H. Frauenfelder, F. Parak and R.D. Young, Annu. Rev. Biophys. Biophys. Chem. 17 (1988) 451 and refs. therein.
6 V.I. Goldanski and Y.F. Krupyanskii, Q. Rev. Biophys. 22 (1989) 39.
7 A. Ansari, J. Berendzen, S.F. Bowne, H. Frauenfelder, I.E.T. Iben, T.B. Sauke, E. Shyamsunder and R.D. Young, Proc. Natl. Acad. Sci. USA 82 (1985) 5000.
8 P.J. Steinbach, A. Ansari, A., L. Berendzen, D. Braunstein, K. Chu, B.R. Cowen, D. Ehrenstein, H. Frauenfelder, J.B. Johnson, D.C. Lamb, S. Luck, J.R. Mourant, G.U. Nienhaus, P. Ormos, R. Philipp, R. Scholl, A. Xie and R.D. Young, Biochemistry 30 (1991) 3988.
9 W.D. Tian, J.T. Sage and P.M. Champion, Phys. Rev. Lett. 68 (1992) 408.
10 S.W. Englander and N.R. Kallenbach, Q. Rev. Biophys. 16 (1984) 521.
11 B. Carling, J. Chem. Phys. 91 (1989) 427.
12 A.E. Garcia, Phys. Rev. Lett. 68 (1992) 2696.
13 H. Frauenfelder, N.A. Alberding, A. Ansari, D. Braunstein, B.R. Cowen, M.K. Hong, I.E.T. Iben, J.B. Johnson, S. Luck, M.C. Marden, J.R. Mourant, P. Ormos, L. Reinisch, R. Scholl, A. Schulte, E. Shyamsunder, L.B. Sorensen, P.J. Steinback, A.H. Xie, R.D. Young and K.T. Yue, J. Phys. Chem. 94 (1990) 1024.
14 M.K. Hong, D. Braunstein, B.R. Cowen, H. Frauenfelder, I.E.T. Iben, J.R. Mourant, P. Ormos, R. Scholl, P.J. Schulte, P.J. Steinbach, A.H. Xie and R.D. Young, Biophys. J. 58 (1990) 429.
15 E.E. Di Iorio, U.R. Hiltpold, D. Filipovic, K.H. Winterhalter, E. Gratton, E. Vitrano, A. Cupane, M. Leone and L. Cordone, Biophys. J. 59 (1991) 742.
16 H. Frauenfelder, in: Amorphous and liquid materials, NATO series, eds. E. Luscher, G. Fritsch and G. Jacucci (Martinus Nijhoff Publishers, Dordrecht 1987), p. 3.
17 H. Frauenfelder, G.A. Petsko and D. Tsernoglou, Nature 280 (1979) 558.
18 J.C. Smith, Q. Rev. Biophys. 24 (1991) 227.
19 R. Elber and M. Karplus, Science 235 (1987) 318.
20 J.R. Alcala, E. Gratton and F.G. Prendergast, Biophys. J. 51 (1987) 925.
21 A. Ansari, J. Berendzen, D. Braunstein, B.R. Cowen, H. Frauenfelder, M.K. Hong, I.E.T. Iben, J.B. Johnson, P. Ormos, T.B. Sauke, R. Scholl, A. Schulte, P.J. Steinback, J. Vittitow and R.D. Young, Biophys. Chem 26 (1987) 337.
22 F. Parak and L. Reinisch, Methods Enzymol. 131 (1986) 568.
23 S. Cusack and W. Doster, Biophys. J. 56 (1990) 243.
24 I.E.T. Iben, B.R. Cowen, R. Sanches and J.M. Friedman, Biophys. J. 59 (1991) 908.
25 V. Srajer, K.T. Schomacker and P.M. Champion, Phys., Rev. Lett. 57 (1986) 1267.
26 A.R. Bizzarri and S. Cannistraro, Appl. Magn. Reson. 2 (1991) 627.
27 F. Parak, H. Hartmann, K.D. Aumann, H. Reuscher, G. Rennekamp, H. Bartunik and W. Steigemann, Eur. Biophys. J. 15 (1987) 237.
28 V. Srajer, L. Reinisch and P.M. Champion, J. Am. Chem. Soc. 110 (1988) 6656.
29 A.R. Bizzarri, Conformational substate distribution in high spin ferric myoglobin as studied by electron paramagnetic resonance, Ph.D. dissertation (SISSA, International School for Advanced Studies, Trieste 1991).
30 A.R. Bizzarri and S. Cannistraro, Biophys. Chem. 42 (1992) 79.
31 A.S. Brill, F.G. Fiamingo and D.A. Hampton, J. Inorg. Biochem. 28 (1986) 137.
32 J.C. Salerno, Biochem. Soc. Trans. 13 (1985) 611.
33 W.R. Hagen, J. Magn. Reson. 44 (1981) 447.
34 C. More, P. Bertrand and J.P. Gayda, J. Magn. Reson. 73 (1987) 13.

35 G. Giugliarelli, P. Tancini and S. Cannistraro, J. Phys. E (Sci. Instrum.) 22 (1989) 702.
36 J.F. Gibson, in: ESR and NMR of paramagnetic species in biological and related systems, eds. I. Bertini and R.S. Drago (D. Reidel, Dordrecht, 1979), p. 225.
37 J. Peisach, W.E. Blumberg, S. Ogawa, E.A. Rachmilewitz and R. Oltzik, J. Biol. Chem. 25 (1971) 3342.
38 M. Kotani, Adv. Quantum Chem. 4 (1968) 227.
39 C.P. Scholes, J. Chem. Phys. 52 (1970) 4890.
40 F.G. Fiamingo, A.S. Brill, D.A. Hampton and R. Thorkildsen, Biophys. J. 55 (1989) 67.
41 J.R. Pilbrow, J. Magn. Reson. 58 (1984) 186.
42 R. Aasa and T. Vanngard, J. Magn. Reson. 19 (1975) 308.
43 A. Isomoto, H. Watari and Kotani, J. Phys. Soc. Jpn. 29 (1970) 1571.
44 S. Cannistraro and G. Giugliarelli, Mol. Phys. 58 (1986) 173.
45 A.S. Brill, Transition metal in biochemistry (Springer-Verlag, New York, 1977).
46 W.R. Hagen, D.O. Hearshen, R.H. Sands and W.R. Dunham, J. Magn. Reson. 61 (1985) 220.
47 W.R. Hagen, W.R. D.O. Hearshen, L.J. Harding and W.R. Dunham, J. Magn. Reson. 61 (1985) 233.
48 A.S. Yang and B.J. Gaffney, Biophys. J. 51 (1987) 55.
49 W. Froncisz and J.S. Hyde, J. Chem. Phys. 73 (1980) 3123.
50 G. Giugliarelli and S. Cannistraro, Il Nuovo Cim. 4 (1984) 194.
51 S. Cannistraro and G. Giugliarelli, Chem. Phys. 98 (1985) 115.
52 A.S. Brill, F.G. Fiamingo, D.A. Hampton, P.D. Levin and R. Thorkildsen, Phys. Rev. Lett. 54 (1985) 1864.
53 S. Kirkpatrick, C.D. Gelatt and M.P. Vecchi, Science 220 (1983) 671.
54 S. Cannistraro, Chem. Phys. Lett. 122 (1985) 165.
55 C.E. Schäffer and C.K. Jorgensen, Mol. Phys. 9 (1965) 401.
56 J.K. Burdett, Molecular shapes—Theoretical models of inorganic stereochemistry (Wiley and Sons, New York, 1980).
57 M. Wolfsberg and L. Helmholtz, J. Chem. Phys. 20 (1952) 837.
58 C.E. Schäffer, Proc. R. Soc. A297 (1967) 96.
59 M. Bacci, Chem. Phys. 40 (1979) 237.
60 J.H.E. Griffith, Theory of transition of metal ions (Cambridge Univ. Press, London, 1961).
61 A. Abragam and B. Bleaney, Electron paramagnetic resonance of transitions ions (Clarendon Press, Oxford, 1970) and refs. therein.
62 T. Takano, J. Mol. Biol. 110 (1977) 569.
63 M. Bacci, Biophys. Chem. 11 (1980) 39.
64 M. Gerloch and R.C. Slade, Ligand-field parameters (Cambridge University Press, London, 1973).
65 F. Parak and E.W. Knapp, PNAS 81 (1984) 7088.
66 W. Nadler, A.T. Brunger, K. Schulten and M. Karplus, PNAS 84 (1987) 7933.
67 M. Bacci and S. Cannistraro, Appl. Magn. Reson. 1 (1990) 369.
68 G.P. Sing, F. Parak, S. Hunklinger and K. Dransfeld, Phys. Rev. Lett. 47 (1981) 685.
69 K. Gekko and S.N. Timasheff, Biochemistry 20 (1981) 4667.
70 S.Y. Gerlma, Eur. J. Biochem. 14 (1970) 150.
71 S.N. Timasheff, J.C. Lee, E.P. Pittz and N. Tweedy, J. Colloid Interface Sci. 55 (1976) 658.
72 J.C. Lee and S.N. Timasheff, J. Biol. Chem. 251 (1981) 523.
73 H. Hori, M. Iketa-Saito and T. Yoketani, Nature 288 (1980) 501.
74 M.R. Ondrias and D.L. Rousseau, Science 213 (1981) 657.
75 G. Astl and E. Mayer, Biochim. Biophys. Acta, 1080 (1991) 155.